

## Nanoscale mechanisms of singlet fission in amorphous molecular solid

Weiwei Mou,<sup>1</sup> Shinnosuke Hattori,<sup>1,a)</sup> Pankaj Rajak,<sup>1</sup> Fuyuki Shimojo,<sup>1,2</sup>  
 and Aiichiro Nakano<sup>1</sup>

<sup>1</sup>*Collaboratory for Advanced Computing and Simulations, Department of Physics and Astronomy, Department of Computer Science, Department of Chemical Engineering and Materials Science, University of Southern California, Los Angeles, California 90089-0242, USA*

<sup>2</sup>*Department of Physics, Kumamoto University, Kumamoto 860-8555, Japan*

(Received 28 November 2012; accepted 26 February 2013; published online 29 April 2013)

Fission of a spin-singlet exciton into two triplet excitons, if realized in disordered organic solid, could revolutionize low-cost fabrication of efficient solar cells. Here, a divide-conquer-recombine approach involving nonadiabatic quantum molecular dynamics and kinetic Monte Carlo simulations identifies the key molecular geometry and exciton-flow-network topology for singlet-fission “hot spots” in amorphous diphenyl tetracene, where fission occurs preferentially. The simulation reveals the molecular origin of experimentally observed two time scales in exciton population dynamics and may pave a way to nanostructural design of efficient solar cells from first principles. © 2013 American Institute of Physics. [<http://dx.doi.org/10.1063/1.4795138>]

Singlet fission (SF) is a process, in which a spin-singlet electron-hole pair (or exciton) in an organic semiconductor is split into two spin-triplet excitons.<sup>1</sup> Fission of a photoexcited singlet exciton may lead to the generation of multiple charge carriers from a single photon. Thus, SF could significantly increase the power conversion efficiency of solar cells.<sup>2</sup> Key to achieving high efficiency is microscopic understanding of photoexcitation dynamics, so that the SF process can be tuned to kinetically out-compete other decay channels. Experimentally, population dynamics of singlet and triplet excitons has been studied by time-resolved two-photon photoemission spectroscopy and other techniques.<sup>3</sup> Quantum-mechanical calculations have suggested an essential role of molecular motions in interpreting measured SF kinetics.<sup>4,5</sup> Namely, molecular dynamics upon photoexcitation modifies intermolecular geometry, which in turn affects the energies of electronic excited states and nonadiabatic coupling between them.

So far, high SF yield has been limited to high-quality molecular crystals.<sup>1</sup> However, this is not compatible with the major advantage of organic solar cells, i.e., inexpensive solution processing such as roll-to-roll printing, which has limited control over the resulting crystallinity. If SF is realized instead in disordered molecular solid that is commonly obtained by mass production techniques, it will have an enormous commercial impact by enabling low-cost fabrication of high-efficiency solar cells. Recently, Roberts *et al.* made an experimental breakthrough by observing SF in amorphous 5,12-diphenyl tetracene (DPT).<sup>6</sup> Their ultrafast transient absorption measurements identified two time constants (1 and 100 ps) in exciton population dynamics. The biexponential decay of singlet excitons was hypothesized to arise from the existence of “SF hot spots,” where SF rates are much higher than those on the other sites.<sup>6</sup> Namely, excitons photoexcited near the hot spots rapidly undergo fission, whereas the fission of those generated elsewhere involves slow diffusion to the hot spots. Now, the central question is:

What is the molecular origin of SF hot spots, if they in fact exist? An answer to this question is indispensable toward nanostructural design of efficient SF-based solar cells.

In contrast to SF in crystals<sup>5</sup> and molecular dimers,<sup>7</sup> SF in amorphous molecular solid has not been studied theoretically. This is largely due to the required large quantum-mechanical calculations that capture nanostructural features. To address this challenge, we adopt a divide-conquer-recombine (DCR) approach, where the divide-and-conquer phase<sup>8–10</sup> constructs globally informed local electronic-structure solutions, which in the recombine phase are synthesized into a global solution conforming to correct symmetry. Specifically, we first perform nonadiabatic quantum molecular dynamics (NAQMD) simulations<sup>11–17</sup> embedded in amorphous DPT, which describe coupled electron-ion dynamics involving nonadiabatic transitions between excited electronic states. Simulation results confirm the existence of postulated SF hotspots and reveal their molecular origin in terms of the geometry of DPT molecular dimers. NAQMD results on phonon-assisted exciton dynamics are then augmented with time-dependent perturbation calculation of SF rates to provide inputs to kinetic Monte Carlo (KMC) simulation<sup>18</sup> of an exciton-flow network in amorphous DPT. The calculated exciton population dynamics exhibits two time scales in conformity with experimental observation.<sup>6</sup> Analysis of the simulation data identifies the key topology of the exciton-flow network for SF hot spots.

An amorphous DPT solid consisting of 6400 atoms (or 128 DPT molecules) is prepared in a cubic simulation box with the side length of 43.3 Å by the melt-quench procedure in molecular dynamics (MD) simulation (see the supplementary material<sup>19</sup>). Periodic boundary conditions are applied in all Cartesian directions. X-ray diffraction data have shown that vapor deposited DPT films are amorphous, unlike crystalline tetracene films prepared under a similar condition.<sup>6</sup> This difference has been attributed to the shape of the DPT molecule in Fig. 1(a). It consists of a four-ringed backbone  $\pi$ -orbital plane identical to that of tetracene, to which two side phenyl groups are attached. The amorphization is likely

<sup>a)</sup>Present address: Sony Corporation, Atsugi, Kanagawa 243-0021, Japan.

due to frustrated crystal growth caused by the side phenyl groups.<sup>6</sup> The amorphous DPT configuration obtained by the MD simulation is shown in Fig. 1(b).

Starting from the amorphous DPT configuration, we perform NAQMD simulations<sup>11–17</sup> to study exciton dynamics. The NAQMD simulations are based on the linear response time-dependent density functional theory<sup>20</sup> to describe electronic excited states and a surface hopping approach<sup>21</sup> to describe transitions between excited states. A series of techniques are employed for efficiently calculating long-range exact exchange correction<sup>22</sup> and excited-state forces. The simulation program is parallelized using hybrid spatial and band decomposition. Detailed description of our NAQMD simulation code is given in Ref. 23. A similar NAQMD approach to exciton dynamics was used by Zhang *et al.* to study exciton diffusion in polymers.<sup>15</sup>

To simulate exciton dynamics in amorphous DPT, we need to move up from the molecular level to the nanostructural level. To enable larger NAQMD simulations than were performed previously (<1000 atoms),<sup>15,16</sup> we employ a divide-and-conquer scheme,<sup>8–10</sup> in which the entire simulation box is subdivided into  $M$  non-overlapping spatial domains  $\Omega_{0i}$ . Here, each DPT molecule constitutes  $\Omega_{0i}$ , thus  $M = 128$ . We augment  $\Omega_{0i}$  by surrounding it with a buffer layer consisting of the  $k$  nearest-neighbor molecules (we use  $k = 2$ ), so that the augmented domains  $\Omega_i$  are mutually overlapping. For NAQMD simulation within each  $\Omega_i$ , the rest of the system is represented by a fixed charge density. (A similar charge patching method<sup>24</sup> was used in large electronic-structure calculations.) Each NAQMD simulation starts from an electronic excited state corresponding to the excitation of an electron from the highest occupied molecular orbital (HOMO) to the lowest unoccupied molecular orbital (LUMO). Each NAQMD simulation is run for 200 fs.

Figure 2 shows snapshots of quasi-electron and quasi-hole charge densities for one of the NAQMD simulations. We observe rapid diffusive motion of the exciton as in Ref. 15. We find that excitons in amorphous DPT are localized within one molecule most time (Figs. 2(a) and 2(d)) except for short period of time ( $\sim$ a few fs) when the exciton hops from one molecule to another (Figs. 2(b) and 2(c)) assisted by molecular motions. This is unlike tetracene and pentacene crystals, in which delocalized excitons extend over  $\sim$ 10 molecules.<sup>5</sup> The exciton localization is quantified by the participation number,<sup>25</sup>  $n_p = 1/\sum_i p_i^2$ . Here,  $p_i$  is the existing

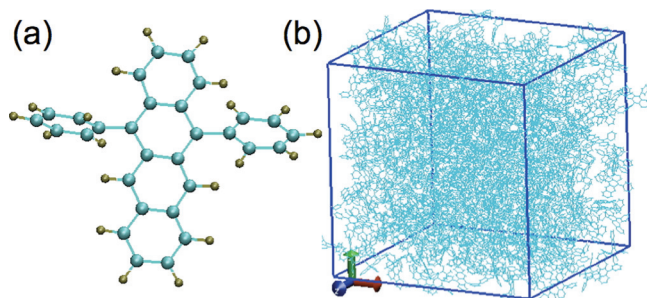


FIG. 1. (a) DPT molecule, where cyan and yellow spheres represent C and H atoms, respectively. (b) Amorphous DPT configuration, where cyan lines represent atomic bonds.

probability of the exciton in the  $i$ th molecule, which is obtained by first projecting the quasi-electron and quasi-hole densities<sup>15</sup> onto the molecule and then averaging the quasi-electron and quasi-hole probabilities. The  $n_p$  value reflects the number of molecules, over which the exciton is spread. Figure 2(e) shows  $n_p$  as a function of time during the NAQMD simulation shown in Figs. 2(a)–2(d). It mostly takes a value near unity, indicating that the exciton is localized on one DPT molecule, except for short transient times when the exciton extends over 2 molecules (i.e.,  $n_p \sim 2$ ). This is consistent with experimental observations, where both optical absorption and emission spectra for vapor deposited DPT films are nearly identical to those in solutions, signifying the highly localized nature of excitons in DPT films.<sup>6</sup>

NAQMD trajectories are analyzed to obtain exciton-hopping rates between DPT molecules. The overlapping domains in the divide-and-conquer approach allow the construction of a graph data structure that spans the entire amorphous DPT solid. In the graph (or exciton-flow network), each DPT molecule constitutes a node, and the nodes are interconnected by directed edges labeled by the corresponding exciton hopping rates obtained by the NAQMD simulations. The nonadiabatic coupling is also used to compute the exciton annihilation rate, at which each exciton recombines

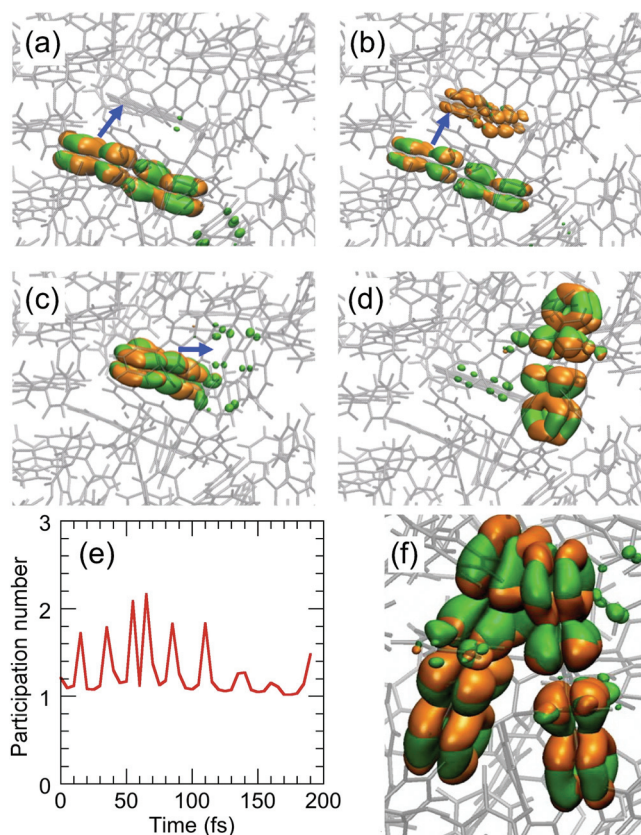


FIG. 2. (a)–(d) Snapshots of an exciton in one of the NAQMD simulations. Isosurfaces of the quasi-electron and quasi-hole charge densities of 0.02 a.u. are shown in orange and green colors, respectively. DPT molecules are represented by gray atomic bonds. Blue arrows indicate exciton-hopping events. (e) Exciton participation number as a function of time during the NAQMD simulation. (f) Spatial distribution of the exciton charge density for one of the SF events, showing the final configuration consisting of two spin-triplet excitons (enhanced online) [URL: <http://dx.doi.org/10.1063/1.4795138.1>].

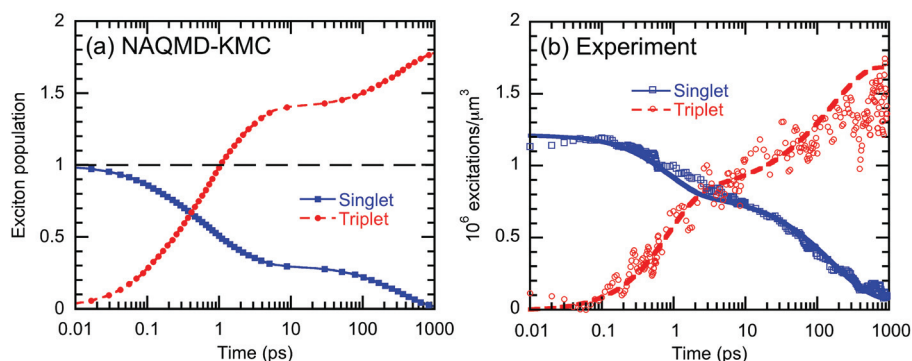


FIG. 3. Time evolution of the population of singlet (blue) and triplet (red) excitons from (a) NAQMD-informed KMC simulation and (b) experiment in Ref. 6.

to the electronic ground state. In addition to the phonon-assisted contribution to electronic transitions computed by NAQMD, we include the spontaneous emission contribution calculated within the transition dipole approximation.<sup>15</sup>

In addition to the exciton hopping and annihilation rates, we estimate the SF rate of each singlet excitonic state using a time-dependent perturbation theory.<sup>26</sup> We use Fermi's golden-rule involving Coulombic matrix elements between initial singlet and final triplet-pair excitonic states.<sup>19</sup> Figure 2(f) shows an example of the final exciton configurations used in these calculations. The SF rate is computed at all time steps during each NAQMD simulation and is time averaged. The calculated SF rates thus incorporate the essential effect of the dynamical change of intermolecular geometry upon photoexcitation as suggested by previous theoretical works.<sup>4,5</sup>

Next, we perform first-principles KMC simulations<sup>18</sup> of exciton dynamics<sup>15</sup> using the calculated hopping rates between DPT molecules as well as the SF and annihilation rates.<sup>19</sup> Each KMC simulation starts by placing an exciton on a randomly selected DPT molecule. At each KMC step, the exciton either (i) hops to one of the  $k$ -neighbor DPT molecules; (ii) splits into two triplet excitons via SF; or (iii) annihilates. The event to occur is chosen stochastically with the probability proportional to the corresponding rate. Each simulation continues until either SF or annihilation event occurs, at which time the number of singlet excitons is decreased by 1. In case of the SF event, in addition, the number of triplet excitons is increased by 2. In total of 5000 KMC simulations are performed to take statistics.

Figure 3(a) shows the calculated population dynamics of singlet and triplet excitons. Our first-principles KMC result captures key features in the experimental data in Ref. 6; see Fig. 3(b). In particular, the NAQMD-informed KMC data reproduce the two time constants observed experimentally. Namely, rapid singlet-exciton decay and triplet-exciton generation occur within  $\sim 1$  ps, followed by slower processes on the time scale of  $\sim 100$  ps. In both simulation and experimental data, the number of generated triplet excitons is larger than that of the initial singlet excitons, signifying efficient SF in amorphous DPT.

The double exponential behavior in Fig. 3 was previously interpreted with an empirical 9-parameter kinetic model that postulates the presence of a subset of molecules only where SF can occur.<sup>6</sup> (The curves in Fig. 3(b) are based on the model with the best-fit parameter values.) Singlet excitons photoexcited near these sites rapidly undergo fission in  $\sim 1$  ps, while those generated elsewhere must diffuse to

these sites via a slow diffusion process. Our first-principles KMC result also exhibits a similar two-stage population dynamics but without any fitting parameter. Analysis of the simulation data confirms the existence of the postulated SF hot spots. Namely, 91% of all the SF events are accounted for by 3.9% of the DPT molecules. This indicates that some dimers of DPT molecules have larger SF rates. We have calculated the SF rate  $k_{\text{SF}}$  averaged over time during the NAQMD simulations for all DPT molecular dimers. The highest and lowest SF rates are  $k_{\text{SF}} = 2.68 \times 10^{12}$  and  $4.35 \times 10^9 \text{ s}^{-1}$ , respectively. The faster SF time constant on the order of 1 ps falls between those in pentacene<sup>27</sup> (80 fs) and tetracene<sup>6</sup> (40–90 ps) films. This is understandable considering the SF reaction energy,  $2\omega_{\text{T}} - \omega_{\text{S}}$ , in these materials ( $\omega_{\text{S}}$  and  $\omega_{\text{T}}$  are the lowest singlet and triplet excitation energies, respectively). The fast SF in pentacene is exergonic with  $2\omega_{\text{T}} - \omega_{\text{S}} = -0.11$  eV, while the slow SF in tetracene is thermally activated with  $2\omega_{\text{T}} - \omega_{\text{S}} = 0.19$ – $0.24$  eV.<sup>6</sup> In DPT,  $\omega_{\text{S}} = 2.46$  eV and  $\omega_{\text{T}} = 1.20$  eV, making SF a weakly exergonic process,  $2\omega_{\text{T}} - \omega_{\text{S}} = -0.06$  eV.<sup>6</sup> Accordingly, the SF time in DPT is intermediate between those in pentacene and tetracene.

To investigate key geometrical features of DPT molecular dimers in SF hot spots, we calculate the translationally and rotationally minimized root mean square displacement (RMSD)<sup>28</sup> between the pair of DPT molecules in each dimer (see Eq. (S5)<sup>19</sup>). The RMSD quantifies geometrical dissimilarity between the two DPT molecules. Figure 4 shows the calculated SF rate as a function of the RMSD. We observe a bimodal distribution of RMSD, one around  $1.96 \pm 0.04$  Å

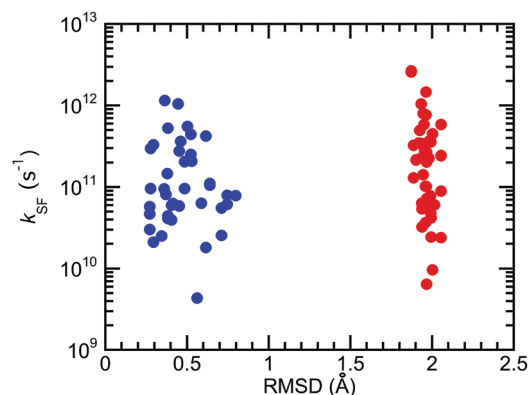


FIG. 4. Calculated SF rates of DPT molecular dimers as a function of the translationally and rotationally minimized RMSD between the molecules. The high- and low-RMSD dimer configurations are colored in red and blue, respectively.

(i.e., high-RMSD dimer configuration) and the other around  $0.47 \pm 0.15$  Å (i.e., low-RMSD dimer configuration). The high- and low-RMSD dimers account for 53.3% and 46.7% of the total dimers, respectively. Among the 3.9% of the dimers that account for 91% of SF events (i.e., SF hot spots), 80% are in high-RMSD configuration. To characterize the geometrical feature that determines the SF rate within the hot spots, we next calculate a geometrical factor  $G$  that represents the distance and relative orientation between the two DPT molecules in each dimer based on a simple dipole-dipole interaction model (Eq. (S6)<sup>19</sup>). Figure S2 shows that the SF rate correlates positively with  $G$ .<sup>19</sup> High SF rates within SF hot spots can be explained by proximity and better alignment of the backbone  $\pi$ -orbital planes in the two DPT molecules in a molecular dimer, which increases dipole-dipole interaction.

Figure 5 shows the geometry of the DPT dimer with the highest SF rate in each set of high- and low-RMSD configurations. The dimer configuration with the highest SF rate is characterized by a parallel stack of the backbone  $\pi$ -orbital planes in short distance. For high-RMSD dimers (Figs. 5(a) and 5(c)), the backbone  $\pi$ -orbital planes are stacked on top of each other. This locates the side phenyl groups of a DPT molecule in close proximity to the other molecule in the dimer. Consequently, the side phenyl groups are more frustrated, causing larger RMSD (Fig. 5(e)). Also, the two DPT molecules are rotated around the stacking direction to form a twisted stack of the backbone  $\pi$ -orbital planes (Fig. 5(c)). This likely reduces the steric repulsion between the side

phenyl groups between the two DPT molecules. For low-RMSD dimers, on the other hand, the backbone  $\pi$ -orbital planes slide away from each other (Figs. 5(b) and 5(d)). In this case, the side phenyl groups are away from the other DPT molecules with less distortion and low RMSD. In summary, SF hot spots are characterized by key geometries of DPT molecular dimers: Twist-stack conformation along with proximity and better alignment of backbone  $\pi$ -orbital planes.

The optimal geometry of molecular dimers for high SF rates has been studied theoretically by Greyson *et al.*<sup>7</sup> In particular, they noted two competing effects of close  $\pi$ -planes: On one hand, it enhances SF according to Eq. (S6);<sup>19</sup> on the other hand, the resulting stronger  $\pi$ -coupling lowers the energy of the lowest excited singlet state, thereby making SF more endergonic and less favorable. Due to the existence of side phenyl groups, balance between these two competing effects in DPT is highly nontrivial. X-ray diffraction study has shown that the DPT crystal consists of two types of cofacial  $\pi$ -plane stacking configurations:<sup>6</sup> Eclipsed stacking, where two  $\pi$ -planes are stacked on top of each other, and staggered stacking. The distance between  $\pi$ -planes is larger for the eclipsed stacking, because the side phenyl groups prevent their close approach. The optimal molecular geometry identified in our simulation of amorphous DPT is intermediate between the crystalline eclipsed and staggered stacking configurations.

In addition to the geometric indicators (RMSD and  $G$ ) for high SF rates, we have found that the topology of the exciton-flow network influences the hot spots. To understand the key network topological feature for SF hot spots, we perform reverse  $k$ -nearest neighbor (RKNN) analysis:<sup>29</sup> To how many other molecules, a given molecule is within the  $k$ th nearest neighbors? Among DPT molecules with high SF rates, Fig. S3 shows positive correlation between the RKNN degree (for  $k = 2$ ) of a DPT molecule with the number of fissions that occurred in the NAQMD-KMC simulation for the molecule.<sup>19</sup> Namely, a molecule with a high RKNN degree acts as a hub of the exciton-flow network, to which a large number of excitons flow into. When a network hub coincides with a high SF-rate site, the site acts as a SF hot spot.

In summary, our DCR approach based on NAQMD and KMC simulations has revealed key molecular dimer geometries (i.e., twist-stack conformation along with proximity and better alignment of the backbone  $\pi$ -orbital planes) and exciton-flow network topology (i.e., large reverse  $k$ -nearest neighbor degree) that facilitate efficient fission of a photoexcited spin-singlet exciton into two triplet excitons in amorphous DPT. The atomistic mechanisms explain the origin of experimentally observed two time scales for SF in amorphous DPT. The design space for efficient SF spans a hierarchy of levels: Single-molecular level (e.g., planarity of the  $\pi$ -orbital plane); stacking geometry of molecular dimers (e.g., denser twist-stack packing); and exciton-flow network topology. Recent experiments hinted that SF may not necessarily be as efficient in crystalline DPT as in amorphous DPT,<sup>30</sup> indicating a highly nontrivial nature of the nanoscopic design across these levels. In this paper, a simple transition dipole model was found to be a good descriptor for local molecular design for efficient fission, together with an exciton flow network analysis. Such atomistic understanding

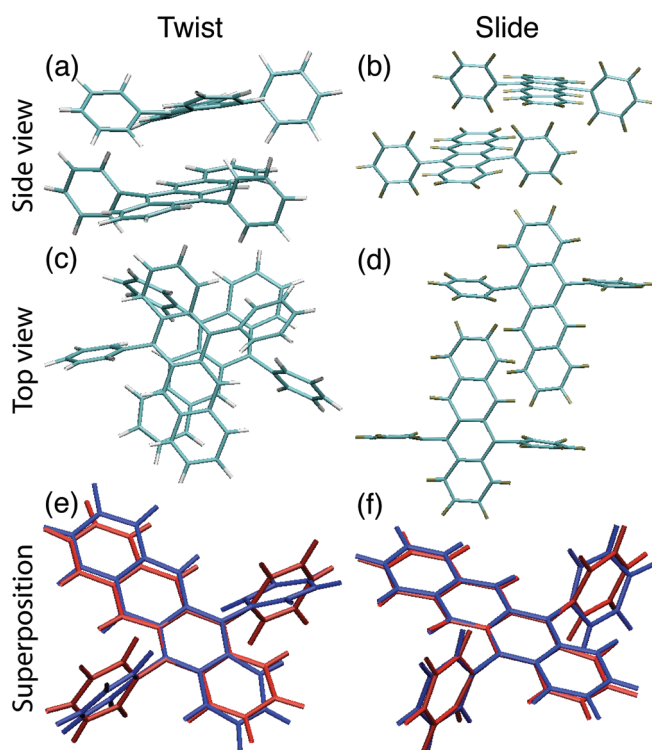


FIG. 5. The geometry of DPT dimers for twist (a and c) and slide (b and d) stacking configurations. Both side (a and b) and top (c and d) views are shown, where lines represent bonds between C (cyan) and H (yellow) atoms. Optimally superposed molecules with the minimal RMSD for the twist and slide pairs are shown in e and f, respectively, where the two molecules in each pair are distinguished by different colors (blue and red).

is expected to augment a kinetic modeling of organic solar cells,<sup>31</sup> thereby paving a way to first-principles, molecular network-level design of efficient solar cells.

We thank S. T. Roberts for providing us with experimental data and K. Nomura for visualization. This work was supported by the U.S. Department of Energy (DOE), Office of Science, under Award DE-FG02-04ER46130. Performance optimization of the simulation code was supported by DOE SciDAC-e Award DE-FC02-06ER25765. W.M. was supported by the Center for Energy Nanoscience, a DOE Energy Frontier Research Center under Award DE-SC0001013.

- <sup>1</sup>M. B. Smith and J. Michl, *Chem. Rev.* **110**(11), 6891–6936 (2010).
- <sup>2</sup>P. J. Jadhav, A. Mohanty, J. Sussman, J. Lee, and M. A. Baldo, *Nano Lett.* **11**(4), 1495–1498 (2011).
- <sup>3</sup>W. L. Chan, M. Ligges, A. Jailaubekov, L. Kaake, L. Miaja-Avila, and X. Y. Zhu, *Science* **334**(6062), 1541–1545 (2011).
- <sup>4</sup>P. M. Zimmerman, Z. Y. Zhang, and C. B. Musgrave, *Nat. Chem.* **2**(8), 648–652 (2010).
- <sup>5</sup>P. M. Zimmerman, F. Bell, D. Casanova, and M. Head-Gordon, *J. Am. Chem. Soc.* **133**(49), 19944–19952 (2011).
- <sup>6</sup>S. T. Roberts, R. E. McAnally, J. N. Mastron, D. H. Webber, M. T. Whited, R. L. Brutchey, M. E. Thompson, and S. E. Bradforth, *J. Am. Chem. Soc.* **134**(14), 6388–6400 (2012).
- <sup>7</sup>E. C. Greyson, B. R. Stepp, X. D. Chen, A. F. Schwerin, I. Paci, M. B. Smith, A. Akdag, J. C. Johnson, A. J. Nozik, J. Michl, and M. A. Ratner, *J. Phys. Chem. B* **114**(45), 14223–14232 (2010).
- <sup>8</sup>W. T. Yang, *Phys. Rev. Lett.* **66**(11), 1438–1441 (1991).
- <sup>9</sup>F. Shimojo, R. K. Kalia, A. Nakano, and P. Vashishta, *Phys. Rev. B* **77**(8), 085103 (2008).
- <sup>10</sup>D. R. Bowler and T. Miyazaki, *Rep. Prog. Phys.* **75**(3), 036503 (2012).
- <sup>11</sup>C. F. Craig, W. R. Duncan, and O. V. Prezhdo, *Phys. Rev. Lett.* **95**(16), 163001 (2005).
- <sup>12</sup>C. P. Hu, H. Hirai, and O. Sugino, *J. Chem. Phys.* **127**(6), 064103 (2007).
- <sup>13</sup>E. Tapavicza, I. Tavernelli, and U. Rothlisberger, *Phys. Rev. Lett.* **98**(2), 023001 (2007).
- <sup>14</sup>S. Meng, J. Ren, and E. Kaxiras, *Nano Lett.* **8**(10), 3266–3272 (2008).
- <sup>15</sup>X. Zhang, Z. Li, and G. Lu, *Phys. Rev. B* **84**(23), 235208 (2011).
- <sup>16</sup>W. Mou, S. Ohmura, F. Shimojo, and A. Nakano, *Appl. Phys. Lett.* **100**(20), 203306 (2012).
- <sup>17</sup>C. Lv, X. J. Wang, G. Agalya, M. Koyama, M. Kubo, and A. Miyamoto, *Appl. Surf. Sci.* **244**(1-4), 541–545 (2005).
- <sup>18</sup>K. A. Fichthorn and W. H. Weinberg, *J. Chem. Phys.* **95**(2), 1090–1096 (1991).
- <sup>19</sup>See supplementary material at <http://dx.doi.org/10.1063/1.4795138> for simulation details.
- <sup>20</sup>M. E. Casida, in *Recent Advances in Density Functional Methods (Part I)*, edited by D. P. Chong (World Scientific, Singapore, 1995), pp. 155–192.
- <sup>21</sup>J. C. Tully, *J. Chem. Phys.* **93**(2), 1061–1071 (1990).
- <sup>22</sup>Y. Tawada, T. Tsuneda, S. Yanagisawa, T. Yanai, and K. Hirao, *J. Chem. Phys.* **120**(18), 8425–8433 (2004).
- <sup>23</sup>F. Shimojo, S. Ohmura, W. Mou, R. K. Kalia, A. Nakano, and P. Vashishta, *Comput. Phys. Commun.* **184**(1), 1–8 (2013).
- <sup>24</sup>N. Vukmirovic and L. W. Wang, *J. Chem. Phys.* **134**(9), 094119 (2011).
- <sup>25</sup>A. Nakano, P. Vashishta, and R. K. Kalia, *Phys. Rev. B* **43**(13), 10928–10932 (1991).
- <sup>26</sup>Y. Fu, Y. H. Zhou, H. B. Su, F. Y. C. Boey, and H. Agren, *J. Phys. Chem. C* **114**(9), 3743–3747 (2010).
- <sup>27</sup>M. W. B. Wilson, A. Rao, J. Clark, R. S. S. Kumar, D. Brida, G. Cerullo, and R. H. Friend, *J. Am. Chem. Soc.* **133**(31), 11830–11833 (2011).
- <sup>28</sup>A. L. Ferguson, A. Z. Panagiotopoulos, P. G. Debenedetti, and I. G. Kevrekidis, *Proc. Natl. Acad. Sci.* **107**(31), 13597–13602 (2010).
- <sup>29</sup>F. Korn and S. Muthukrishnan, *ACM SIGMOD Rec.* **29**(2), 201–212 (2000).
- <sup>30</sup>S. T. Roberts, private communication (2013).
- <sup>31</sup>N. C. Giebink, G. P. Wiederrecht, M. R. Wasielewski, and S. R. Forrest, *Phys. Rev. B* **82**(15), 155305 (2010).